Medical Image Segmentation Using Minimal Path Deformable Models With Implicit Shape Priors

Pingkun Yan, *Member, IEEE*, and Ashraf A. Kassim, *Member, IEEE*

Abstract—This paper presents a new method for segmentation of medical images by extracting organ contours, using minimal path deformable models incorporated with statistical shape priors. In our approach, boundaries of structures are considered as minimal paths, i.e., paths associated with the minimal energy, on weighted graphs. Starting from the theory of minimal path deformable models, an intelligent "worm" algorithm is proposed for segmentation, which is used to evaluate the paths and finally find the minimal path. Prior shape knowledge is incorporated into the segmentation process to achieve more robust segmentation. The shape priors are implicitly represented and the estimated shapes of the structures can be conveniently obtained. The worm evolves under the joint influence of the image features, its internal energy, and the shape priors. The contour of the structure is then extracted as the worm trail. The proposed segmentation framework overcomes the shortcomings of existing deformable models and has been successfully applied to segmenting various medical images.

Index Terms—Deformable models, energy minimization, medical image segmentation, minimal path, shape prior modeling.

I. INTRODUCTION

SEGMENTATION of anatomical structures is a fundamental operation in medical image analysis. In recent years, computer-vision-based segmentation techniques that combine deformable models with local edge or feature extraction have achieved considerable success in medical image segmentation [1], [2]. With given initial contours, deformable models are able to evolve to obtain the organ boundaries. The starting contours are usually manually initialized as polygons near the actual organ contours.

Deformable models were first introduced into computer vision by Kass *et al.* [3] as "snakes" or active contours, which are now more well known as *parametric deformable models* as they are explicitly represented as parameterized contours in a Lagrangian framework. Although they have been used extensively in medical image segmentation, one of their main difficulties is the inability to adapt to complex topologies. *Geometric deformable models* [4]–[6], or level set methods [7], [8], on the other hand, are represented implicitly as level sets of Lipchitz functions and evolve in an Eulerian fashion. Compared with parametric deformable models, geometric deformable models are superior in many respects, especially in handling topolog-

ical changes. During the past decade, various medical image segmentation methods based on level set methods have been proposed [9].

Although these methods are very powerful in solving object segmentation problems, they have some drawbacks. Deliberate initialization is required by most segmentation methods. Currently, manual initialization is the most commonly used method for deformable models. This becomes impractical when dealing with large numbers of medical images. In addition, initialization may be tedious when dealing with several adjacent objects. Another main drawback is that the current deformable models are computationally complex, requiring a large number of iterations. To deal with these problems, we propose a *minimal path deformable model* based segmentation framework, which is inspired by following work. Cohen *et al.* [10] introduced the minimal path deformable model, which requires only two endpoints and the final contour obtained will be between these two points. This work was further extended in [11] by incorporating the *fast marching* method [8]. On the basis of these works, Han *et al.* [12] developed a minimal path finding algorithm, which eliminates the "metrication errors" by using a "wriggling" process. However, the algorithm easily gets into a local minima during the wriggling process. Hence, a more robust minimal path finding algorithm is needed.

When segmenting or localizing an anatomical structure, prior knowledge is usually very helpful. The incorporation of specific prior information into the deformable models has received great attention. Several methods of incorporating prior shape information into boundary determination have been developed. Cootes *et al.* [13] propose an *active shape model* to construct a statistical shape model from a set of training images for image segmentation. The model is built by outlining the contours and finding point correspondences across shapes. Staib and Duncan [14] incorporate global shape information into the segmentation process by using an elliptic Fourier decomposition of the boundary and placing a Gaussian prior on the Fourier coefficients. In [15], Leventon *et al.* incorporate statistical shape influence into the evolution process of geodesic active contours [6] by attracting the evolving contour toward the shape priors. The correspondence problem is solved in their approach by embedding the prior shape as the zero-level set of a level set function map. Chen *et al.* [16] propose a variational method that minimizes an energy functional defined by the image gradients and the shapes of interest. However, incorporating *a priori* shape knowledge into these approaches is difficult.

In this paper, we present a new minimal path deformable model, which incorporates shape prior knowledge for medical image segmentation. A minimal path deformable model [17]

is used to extract organ boundaries under the influence of shape priors. In our algorithm, the minimal path is evaluated jointly over two weighted graphs. One of the weighted graphs is computed from the image to be segmented and the other is obtained as a signed distance map by implicitly representing the shape prior as its zero-level set. Since the implicit representation is in a very similar form as the weighted graph of the image, the prior shape knowledge is naturally incorporated into the segmentation process. To avoid being trapped by a local minima, our algorithm uses an intelligent "worm" to look for the minimal path. In general, existing minimal path finding algorithms need two or more initialization points, whereas our algorithm requires only a single starting point to obtain a contour. Our work is different from the traditional graph-searching-based contour detection methods (such as [18] and [19]) as it takes into account the properties of the contours and the *a priori* shape knowledge in addition to image features.

This paper is organized as follows. Section II explores the relationship between the original deformable models and the proposed work and then provides and discusses the method for obtaining *a priori* shape knowledge. In Section III, we describe the proposed minimal path deformable model and shape-prior-based segmentation method. Experimental results are presented and discussed in Section IV. Finally, conclusions are summarized in Section V.

II. MINIMAL PATHS AND SHAPE PRIORS

A. Minimal Path Deformable Model

Since the introduction of the parametric deformable model (i.e., "snake") by Kass *et al.* [3], deformable models have been often used to integrate boundaries and extract features from images. In the original parametric deformable models [3], the energy functional $E(\mathcal{C})$ is defined as

$$E(\mathcal{C}) = \int_0^1 \left(\alpha \left| \frac{\partial \mathcal{C}}{\partial s} \right|^2 + \beta \left| \frac{\partial^2 \mathcal{C}}{\partial s^2} \right|^2 - \gamma f(\mathcal{C}(s)) \right) ds \quad (1)$$

where $\mathcal{C}(s)$ is a curve parameterized by $s \in [0, 1]$, α, β, and γ are real positive constants, and f is an edge map of the image. The first two terms on the right side of (1) represent the internal energy, which controls the smoothness of the contours to be detected. The third term is the external energy, which is responsible for attracting the contour toward the object boundaries in an image. Solving (1) for a given set of α, β, and γ amounts to finding the curve $\mathcal{C}$ that minimizes the energy functional $E(\mathcal{C})$. A problem with the original deformable models is the need to select parameters that control the tradeoff between smoothness and proximity to the object. Inappropriate parameters can make the minimization process difficult or even impossible. Caselles *et al.* [6] proved that curve smoothing is obtained by setting $\beta = 0$, which reduces (1) to

$$E(\mathcal{C}) = \alpha \int_0^1 \left| \frac{\partial \mathcal{C}}{\partial s} \right|^2 ds - \gamma \int_0^1 f(\mathcal{C}(s)) \, ds. \quad (2)$$

If $g : [0, +\infty[\to \mathbb{R}^+$ denotes a strictly decreasing function such that $g(r) \to 0$ as $r \to +\infty$, (2) can be changed into a general
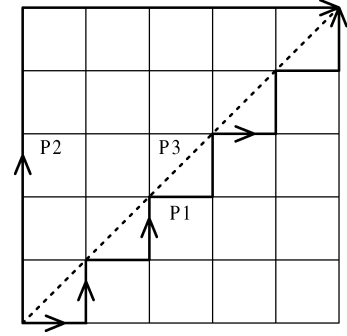

Fig. 1. Illustration of metrication errors.

energy functional by replacing the edge map f with $g(|\nabla I|)^2$

$$E(\mathcal{C}) = \alpha \int_0^1 \left| \frac{\partial \mathcal{C}}{\partial s} \right|^2 ds + \gamma \int_0^1 g(|\nabla I(\mathcal{C})|)^2 ds \quad (3)$$

where ∇I is the gradient of the image $I : [0, a] \times [0, b] \to \mathbb{R}^+$. Minimizing (3) is equivalent to a problem of geodesic computation in a Riemannian space [6]

$$E(\mathcal{C}) = \int_0^1 g(|\nabla I(\mathcal{C})|) \left| \frac{\partial \mathcal{C}}{\partial s} \right| ds. \quad (4)$$

Noting that the Euclidean length of the contour $\mathcal{C}$ is given by

$$L(\mathcal{C}) = \int_0^1 |\mathcal{C}_s| \, ds \quad (5)$$

and the object contour is approached by curve $\mathcal{C}$ so the energy functional $E(\mathcal{C})$ is minimized. Therefore, the problem of image segmentation is transformed into a search for the global minimal path weighted by $g(|\nabla I(\mathcal{C}(s))|)$. Thus, object contours can be delineated by evaluating the minimal paths instead of minimizing the energy $E(\mathcal{C})$ in (1). Methods based on this approach are known as minimal path deformable models, which have lower computational complexity in high-order gradients and do not involve minimizing the corresponding Euler–Lagrange equation.

B. Weighted Graph From Image

The problem of finding the shortest path has been well studied and many excellent algorithms, like Dijkstra's method and dynamic programming [20], have been proposed. These graph searching algorithms can be used for image segmentation, but suffer from metrication errors (see Fig. 1) for several reasons [10]. If pixels are thought of as nodes, a raster image can be considered as a regular graph with unit weights on every link. In addition, the distance between two points is restricted to be a city block distance in graph searching algorithms. Under such an assumption, both P1 and P2 are shortest paths in Fig. 1. However, by refining the graph grids, only P1 can approach the ideal shortest path P3 based on Euclidean distances. In two dimensions (2D), the Euclidean distance between points
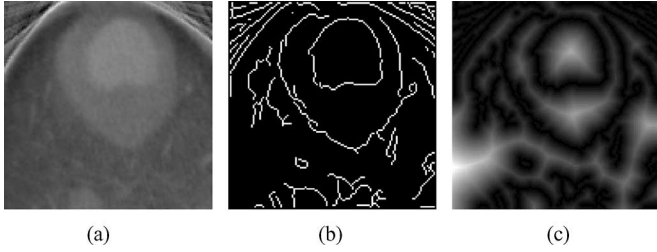
Fig. 2. (a) Sample of CT cardiac image, (b) edge map of the image (result of edge detection), and (c) weighted graph map produced by applying distance transform on the edge map.

(x_1, y_1) and (x_2, y_2) is

$$D = \sqrt{(x_1 - x_2)^2 + (y_1 - y_2)^2}.$$

If the graph in Fig. 1 is weighted as the Euclidean distance map to the starting point, longer paths like P2 will be excluded by a shortest path finding algorithm.

Thus, the Euclidean distance transform [21] can be used to obtain the weighted graphs for the raster images. Since our objective is to extract organ contours, which are normally defined by edges, we expect that the graph nodes have lower weights when they are near the edges and higher weights when far away. Thus, the Euclidean distance transform is applied on the edge map of the image to assign weights to the graphs. For each pixel in the transformed map, the Euclidean distance transform assigns a number that is the distance between that pixel and the nearest nonzero pixel of the edge map. Fig. 2 shows the steps of getting the weighted graph of an image.

C. Prior Shape Modeling

Prior shape knowledge is very useful when segmenting organs from medical images. To incorporate this prior information into the segmentation process, we consider a probabilistic approach and compute a prior on shape variation with a set of given training instances. To build the shape model, we choose a representation of shapes and then define a probability density function over the parameters of the representation.

Suppose that we have a training set $\mathbf{C} = \{\mathcal{C}_i \mid i = 1, 2, \ldots, n\}$ of n registered shapes. To avoid the point correspondence problem in [13], an implicit representation of shapes is desired. Given the selected graph weighting method in our algorithm, it will be convenient to add this prior shape information into the segmentation process if the shapes can be represented as some form of Euclidean distance map. One way is to represent a curve $\mathcal{C}$ by its Euclidean distance transform map Φ : $[0, a] \times [0, b] \to \mathbb{R}^+$, where $\mathcal{C} = \{(x, y) \mid \Phi(x, y) = 0\}$. However, the shape prior model is difficult to derive under this representation due to the discontinuity of function Φ on the curves. To overcome this problem, a curve $\mathcal{C}$ is represented by its signed Euclidean distance transform map $\Psi : [0, a] \times [0, b] \to \mathbb{R}$, where $\mathcal{C} = \{(x, y) \mid \Psi(x, y) = 0\}$ and Ψ has negative values inside $\mathcal{C}$ and positive values outside $\mathcal{C}$, as shown in Fig. 3. With this operation, the shape priors are actually represented by a kind of level set function and own numerous advantages of level sets [9].
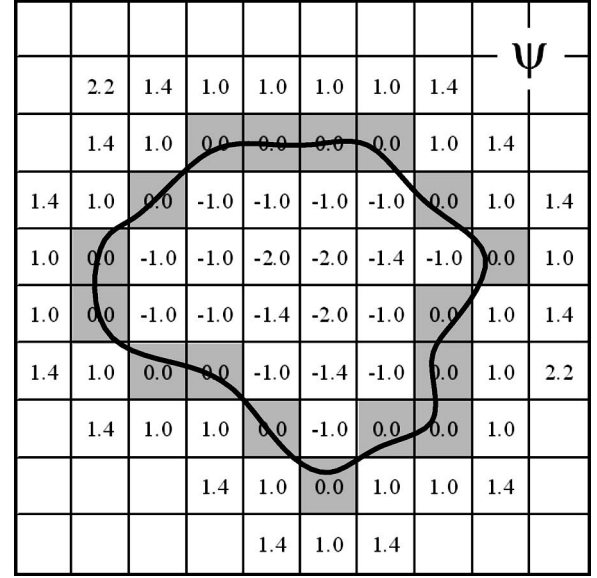

Fig. 3. Object shape is represented implicitly as the zero-level set of its signed distance transform map Ψ.

When building the prior shape model, each curve $\mathcal{C}_i$ in the training set is represented implicitly by the zero-level set of its signed distance map Ψ_i. The mean and variance of the training data can be computed using principal component analysis (PCA) [15]. Subtracting the mean shape $\bar{\Psi} = (1/n) \sum_{i=1}^{n} \Psi_i$ from each Ψ_i and reshaping the differences results column vectors in a $(a \cdot b) \times n$ dimensional matrix $\mathbf{P}$. Using singular value decomposition (SVD), the matrix is decomposed as $\mathbf{P} = \mathbf{U}\boldsymbol{\Sigma}\mathbf{V}^T$. Matrix $\mathbf{U}$ is the model with orthogonal column vectors that consist of the modes of shape variation and diagonal matrix $\boldsymbol{\Sigma}$ is composed of corresponding singular values, i.e., mode amplitudes. An estimate of the object shape can be represented by k principal components and a k-dimensional vector of shape parameters $\mathbf{b}$ (where $k < n$) [15] as

$$\hat{\Psi} = \mathbf{U}_k \mathbf{b} + \bar{\Psi}. \tag{6}$$

Under the assumption of a Gaussian distribution of the shape represented by $\mathbf{b}$, we can compute the probability of a certain curve as

$$p(\mathbf{b}) = \frac{1}{\sqrt{(2\pi)^k |\boldsymbol{\Sigma}_k|}} \exp\left(-\frac{1}{2}\mathbf{b}^T \boldsymbol{\Sigma}_k^{-1} \mathbf{b}\right) \tag{7}$$

where $\boldsymbol{\Sigma}_k$ contains the first k rows and k columns of $\boldsymbol{\Sigma}$.

Fig. 4 shows a sequence of computed tomography (CT) cardiac images over a cardiac cycle [22]. These 15 images are used as the training set. The corresponding manual segmentation results are shown in Fig. 5, based on which the prior shape model is built. The generated shapes with varying modes are shown in Fig. 6 by extracting the zero-level sets from the generated maps. The mean shape and primary modes appear to be reasonable representations of the samples being learned. In Fig. 6, varying the first mode significantly changes the size of the generated shape, while the second and third modes have a rather small influence on the shapes.
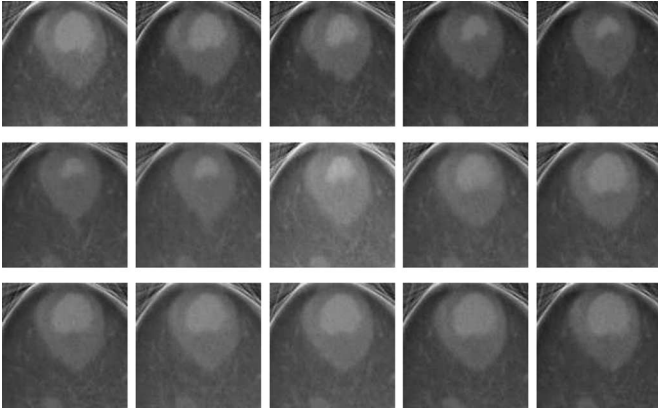
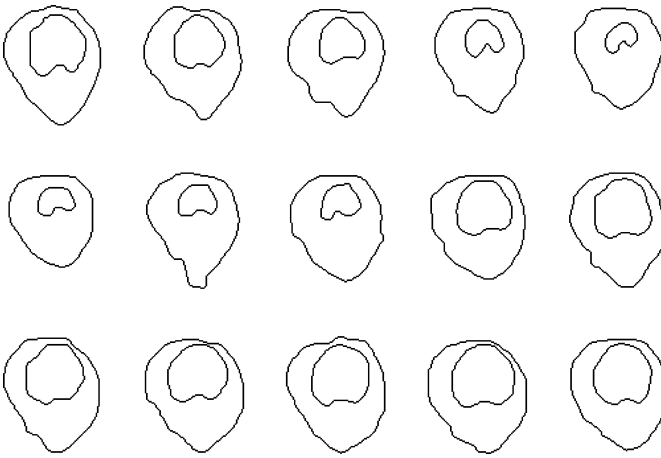Fig. 4.   Samples of CT cardiac image over a cardiac cycle [22].

Fig. 5.   Manual segmentation results of images shown in Fig. 4.

(a) $-2\sigma_1$	(b) $-\sigma_1$	(c) Mean shape $\bar{\Psi}$	(d) $+\sigma_1$	(e) $+2\sigma_1$
(f) $-2\sigma_2$	(g) $-\sigma_2$	(h) Mean shape $\bar{\Psi}$	(i) $+\sigma_2$	(j) $+2\sigma_2$
(k) $-2\sigma_3$	(l) $-\sigma_3$	(m) Mean shape $\bar{\Psi}$	(n) $+\sigma_3$	(o) $+2\sigma_3$

Fig. 6.   Extracted zero-level set of the largest three modes of variation.

III. MINIMAL PATH FINDING

Our goal is to find a single contour that best fits the boundary of a given object of interest. Given that the weighted graph map of the image has lower values near the edges or features, segmentation can be done by looking for a minimal path on it, as discussed in Section II-A. Our algorithm finds the minimal path from a single starting point, using an extended version of our earlier worm algorithm [17].

A. Worm Algorithm

The worm for minimal path detection is composed of a sequence of points and has a length L_w and energy E_w. The edges obtained along an object contour may not be continuous. So, the worm needs to be long enough to skip disjointed parts. As the worm needs to avoid the local minima, its energy consists of both the external energy, which is based on the influence of image features and the prior shape model, and the internal energy generated by its own topology. In this paper, only edges are used as the image features for simplicity although more complicated features can be used to further improve the performance. At each step, the worm compares all the possible ways ahead and moves itself along the one with minimal energy.
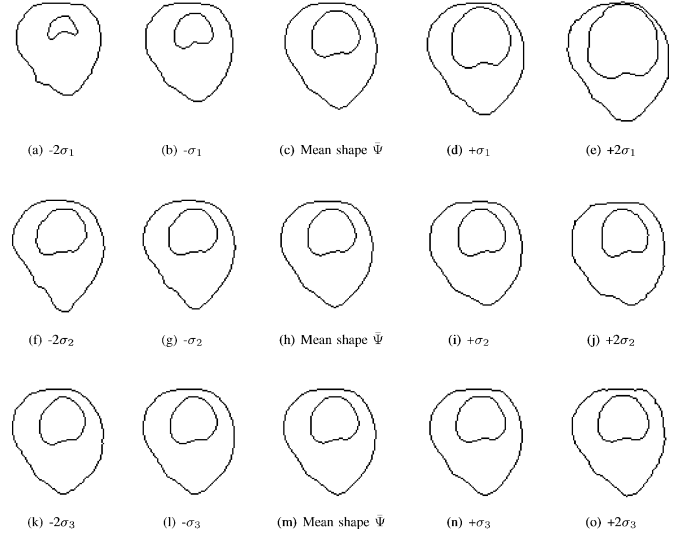
Let F_{shape}, F_{image}, and F_{int} denote the prior shape attraction force, the image feature attraction force, and the internal force acting on the worm, respectively. The force F_{shape} represents the influence from the organ shape estimate produced by the maximum *a posteriori* (MAP) prior shape estimator, which is described in Section III-B. F_{image} describes the force characterized by the weighted graph of the image, while F_{int} tries to stretch the worm body and to keep it from twisting. The overall energy E_w of the worm is then defined as

$$E_{\text{w}} = \int_{\Omega} (\alpha F_{\text{shape}}(\omega) + \beta F_{\text{image}}(\omega) + F_{\text{int}}(\omega))\, d\omega \qquad (8)$$

where $d\omega$ is a small part of the worm body, Ω denotes the extent of the worm body, and α and β are positive real numbers that balance the forces.

In our proposed algorithm, F_{image} is the force that attracts the worm to the edges of the image. It is stronger when the worm is further away from the edges. The edges are detected by Canny edge detector [23] and the distance transform [21] is applied on the edge map, which is used to represent F_{image}, as shown in Fig. 2.

F_{shape} is defined in a similar way as F_{image}. It becomes progressively weaker when the worm is nearer the prior shape, so that this force attracts the worm to the prior shape estimate of the organ according to (8). Since the estimated shape is embedded as the zero-level set in its signed distance map Ψ as shown in Fig. 3, F_{shape} is represented using $|\Psi|$, i.e., the Euclidean distance transform of the shape estimate.

The internal force F_{int} is used to constrain the bending of the worm. This makes the worm robust to noise and prevents it from twisting. It is defined as

$$F_{\text{int}}(\omega) = \gamma(\omega) \left| \frac{\partial^2 \mathcal{C}(\omega)}{\partial s^2} \right|^2 \qquad (9)$$

where $\mathcal{C}(\omega)$ is the body of the worm. In addition

$$\gamma(\omega) = \begin{cases} \gamma_1 & \text{if } F_{\text{image}}(\omega) \le 0.5, \\ \gamma_2 & \text{if } F_{\text{image}}(\omega) > 0.5, \end{cases} \quad \text{where } \gamma_1 \ll \gamma_2. \tag{10}$$

In (10), $F_{\text{image}} \le 0.5$ when the worm is at or very near to an edge. To help the worm fit itself into a complex object shape, F_{int} should be insignificant at edges corresponding to the object contour. In almost all of our numerical calculations, we generally select $\gamma_1 = 0.1$ and $\gamma_2 = 1.0$.

Since raster images can be considered as graphs with rectangular grids, the problem is transformed to graph searching, and dynamic programming [20] is employed to select the minimal path. Dynamic programming was introduced to iteratively optimize deformable models by Amini *et al.* [24]. It requires a large amount of memory and has high computational complexity. The complexity of the algorithm is $O(n \cdot m^2)$, where n and m are the numbers of states and stages, respectively. In Amini *et al.*'s model, the number of states $n = 4$ if the 4-neighbor system is used and the number of stages m equals to the length L of the longest possible contour. So the complexity of the model is $O(L^2)$. In our algorithm, the worm goes forward step by step. At each step, it searches for the best path and moves itself along the path. We record the worm trail as the organ contour. The dynamic programming technique is used when the worm searches its path. Since going back is not allowed for the worm, the number of states $n = 3$. The number of stages m is fixed as the length L_{w} of the worm body. The total number of steps is the length L' of the contour. Thus, the overall computational complexity of our algorithm is $O(L' \cdot L_{\text{w}}^2)$. Since $L' \le L$ and L_{w} is a fixed number, which is no more than 10 in most cases, the complexity of our algorithm is $O(L' \cdot L_{\text{w}}^2) \sim O(L)$. Thus, our algorithm has a much lower computational complexity. The reduction is more significant when dealing with bigger objects, since L becomes larger.

B. MAP Shape Estimation

To incorporate the influence of prior shape model to the contour detection process, the shape of each organ must be correctly estimated. Let Ψ denote the weighted graph that contains the estimated curve of the object. At each step of the curve evolution, the graph Ψ is estimated by

$$\Psi_{\text{MAP}} = \operatorname*{argmax}_{\Psi} p(\Psi \mid \mathcal{C}, G(I)) \tag{11}$$

where $\mathcal{C}$ is the current curve and $G(I)$ denotes the weighted graph of the image I. To compute the MAP shape representation, we expand (11) using Bayes' Rule

$$p(\Psi \mid \mathcal{C}, G(I)) = \frac{p(\mathcal{C} \mid \Psi)p(G(I) \mid \mathcal{C}, \Psi)p(\Psi)}{p(\mathcal{C}, G(I))}. \tag{12}$$

The normalization term in the denominator of (12) can be ignored since it does not depend on the estimated shape of the object. Other terms are defined separately as follows. The first term $p(\mathcal{C} \mid \Psi)$ of (12) represents the probability of existence of a
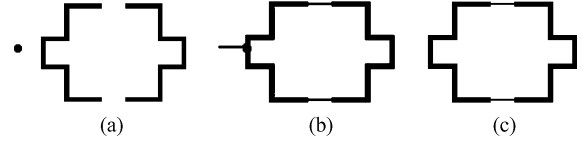

Fig. 7. (a) Use of the worm algorithm for the synthetic image with sharp corners and two breaks. The dot indicates the starting point. (b) The worm stops at the intersection point. (c) Final contour detection result.

curve $\mathcal{C}$, given the estimated shape representation Ψ. Note that this term does not include any image information whatsoever. This term is modeled as a Laplacian density function over the energy of the evolving curve with $|\Psi|$ as its weight map

$$p(\mathcal{C} \mid \Psi) = \exp\left(-\lambda_1 \int_{\mathcal{C}} |\Psi(\mathcal{C}(s))| \, ds\right). \tag{13}$$

The second term in the numerator of (12) computes the probability of seeing certain weighted graph $G(I)$, given a curve $\mathcal{C}$ and an estimated curve representation Ψ. Since object contours usually exist in detected edges, we would expect that the estimated shapes also lie on those edges. Thus, this term can be modeled as a Laplacian density function of the degree of matching the shape estimate to the edges in the image

$$p(G(I) \mid \mathcal{C}, \Psi) = \exp\left(-\lambda_2 \int_{\Psi=0} G(x, y) \, dx \, dy\right). \tag{14}$$

The last term in the numerator of (12) represents the probability of the estimated shape Ψ, which is described earlier in Section II-C. The prior shape estimator is a Gaussian model over the shape parameters α with shape variance $\boldsymbol{\Sigma}_k$

$$p(\Psi) = p(\mathbf{b}) = \frac{1}{\sqrt{(2\pi)^k |\boldsymbol{\Sigma}_k|}} \exp\left(-\frac{1}{2} \mathbf{b}^T \boldsymbol{\Sigma}_k^{-1} \mathbf{b}\right). \tag{15}$$

Putting these into (12) and taking the negative log, we have

$$\Psi_{\text{MAP}} = \operatorname*{argmin}_{\Psi} \left\{ \lambda_1 \int_{\mathcal{C}} |\Psi(\mathcal{C}(s))| \, ds \right.$$
$$\left. + \lambda_2 \int_{\Psi=0} G(x, y) \, dx \, dy + \frac{1}{2} \mathbf{b}^T \boldsymbol{\Sigma}_k^{-1} \mathbf{b} \right\}. \tag{16}$$

Using the MAP shape estimator in (16), the prior shape of the object can be obtained. The MAP shape estimate is reestimated after a number of evolution steps.

IV. RESULTS AND DISCUSSION

When our algorithm is applied on the synthetic image as shown in Fig. 7, it is clearly able to delineate sharp corners and connect disjointed parts to obtain a closed contour. At each step, the worm searches all the possible paths within a range defined by its body length and chooses the shortest one (the worm is not shown in the figure). In addition, the worm has much lower internal energy when it is on or near the edges. These characteristics help the worm fit into sharp corners. Starting

from the red point at the left side of the room in Fig. 7(a), the worm stops when the curve is closed (i.e., self-intersection is detected), as shown in Fig. 7(b). However, the worm trail is not naturally the desired object contour as the starting point is not initialized on the contour. We need to detect the point from which the path begins to be the actual object contour. The closed object contour is obtained as shown in Fig. 7(c).

In the proposed object contour detection scheme, shape priors are first represented implicitly as the zero-level set of their signed distance transform maps and then a statistical shape model is built by computing $\mathbf{U}$ and $\boldsymbol{\Sigma}$, as discussed in Section II-C. A worm starts from an initial point, moves along the minimal path under the influence of image force, its internal force, and shape prior force, and finally stops when the curve is closed. Shape estimates are generated according to image information and the worm trail using the MAP framework as demonstrated in (16). The final segmentation results are obtained by finding the intersection point and removing the worm trail before this point.

To reduce the complexity of our algorithm, of the four parameters α, β, λ_1, and λ_2, we fix $\beta = 1.0$ in (8), which implies that the image force has equal influence as the internal force on the evolution of the worm. We further set $\lambda_1 = 0.1$ and $\lambda_2 = 0.5$ in (16). With this setting, the shape priors have a major impact on the shape estimate, while the evolving worm trail contributes the least since it is only a part of the object contour. Then, in our experiments, we just need to adjust parameter α in (8) to control the influence of shape prior.

Experiments on more than ten sets of medical images are carried to demonstrate the performance of the proposed segmentation method. The evolution of the worm algorithm on a typical 512×512 image takes no more than 0.1 s on a P4 1.8-GHz computer. Fig. 8 shows the segmentation process of a CT cardiac image [22]. Segmentation results without using shape priors are first presented in Fig. 8(c), where the endocardium wall is extracted successfully while only part of the epicardium wall is obtained because no obvious edge information can be found. The situation is improved when shape estimates are considered. Fig. 8(d)–(i) shows the segmentation process of our segmentation method in six steps. In our experimental results, thin curves indicate shape estimates and thick curves represent segmentation results. When the edge information is weak, the shape estimate will guide the worm. In Fig. 8(h), we can see that the shape estimate of the endocardium wall is not very accurate since this image is quite different from the images in our training set. But the worm can still get the correct contour because the edge information is strong there. Thus, the worm does not totally rely on either the image information or the shape information. It balances the influence of image features and prior shape and manages to obtain a better solution. The manual segmentation result [see Fig. 8(j)] is included for comparison.

In another experiment, the magnetic resonance (MR) T1 brain images [25] are segmented. Two sets of segmentation results are shown in Fig. 9. From the second column of Fig. 9, we can see that the edges of the object of interest are disconnected and are sometimes connected with other edges. Although the worm has
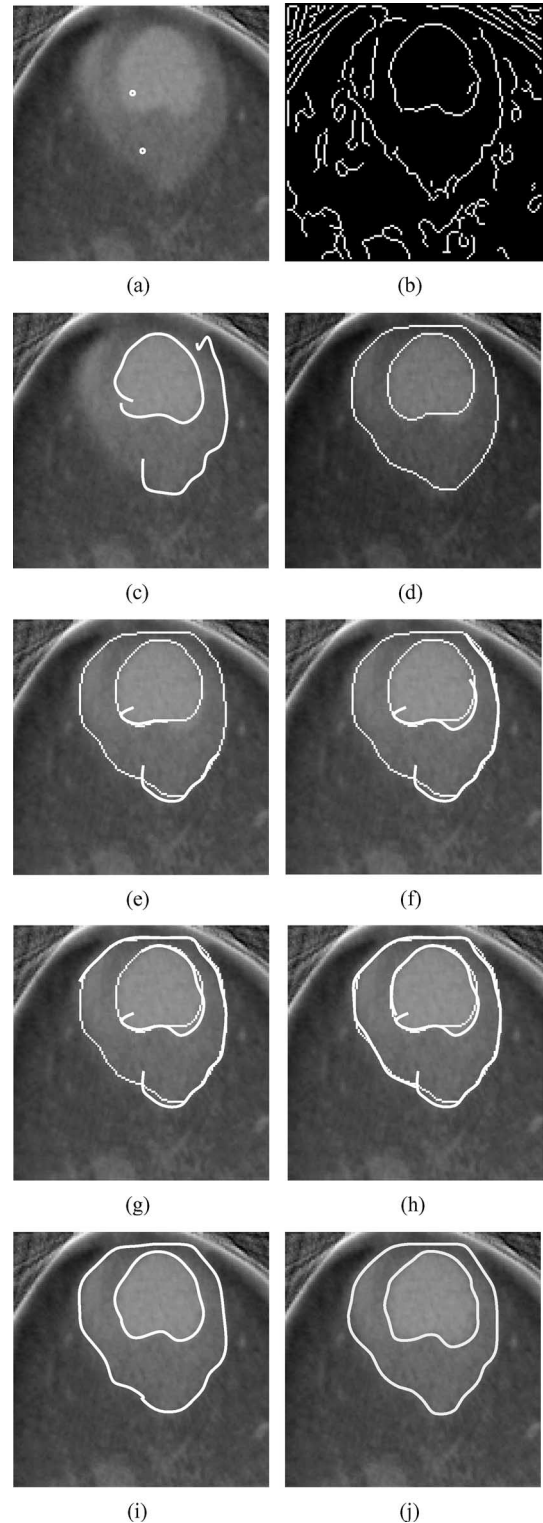

Fig. 8. (a) Segmentation process for CT cardiac image with two initial points, where $\alpha = 0.6$ for the epicardium wall and $\alpha = 0.2$ for the endocardium wall. (b) Detected edges. (c) Segmentation results without prior shape influence. (d) Initial shape estimates. (e)–(h) Intermediate segmentation results. (i) Final segmentation results. (j) Manual segmentation results.

the ability to skip breaks and join the disconnected parts, it is a very challenging task in that the worm can be easily "misled" by other salient edges. But with the aid of prior shape knowledge, the contours are successfully obtained, as shown in the fourth

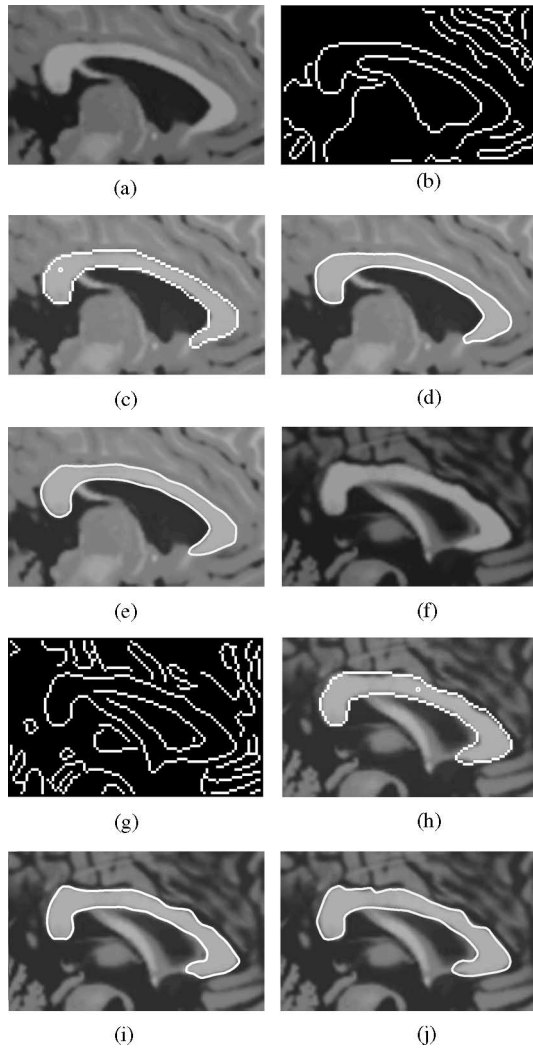Fig. 9.   Segmentation results on MR brain images. In both experiments, we set $\alpha = 0.8$. The first and the second rows show the segmentation processes for data set one and data set two, respectively. (First column) Original images. (Second column) Edge maps. (Third column) Starting points and initial shape estimates. (Fourth column) Final segmentation results. (Fifth column) Manual segmentation results.

column of Fig. 9. Manual segmentation results are provided in the fifth column of Fig. 9 for comparison.

To validate the results, the mean distance error is adopted as a metric to measure the difference between our segmentation results and the ground truth, i.e., manual segmentation results obtained by radiologists. By using this metric, the effect of varying parameter α is shown in Fig. 10. It can be seen that for both data sets the largest error occurs when $\alpha = 0$, which means no shape prior is used. By increasing the value of α, which means by involving the shape prior more and more in the segmentation, the mean distance error gradually decreases and reaches a minimum point. Thus, the best balance between shape prior, image force, and internal force is achieved. It is noted that when we continue to increase the weight of the shape priors, however, the segmentation performance begins to degrade because the shape of the structure is not accurately estimated, which causes errors when the shape prior becomes dominant with large α.
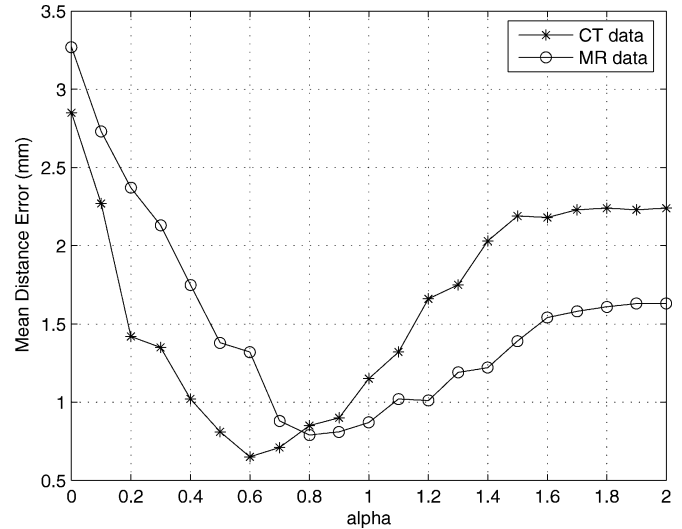

Fig. 10.   Effect of varying parameter α on the segmentation errors.

V. Conclusion

In this paper, we propose a segmentation scheme that extracts object boundaries by finding a path associated with minimal energy. Segmenting organs from an image is then solved by finding the minimal path. An intelligent worm algorithm is used to search the minimal path from a single starting point on a weighted graph. The worm can track complex topologies and link discontinued parts of object contour. To make it less sensitive to the detected edges, an implicit prior shape model is incorporated as a weighted graph and a more robust segmentation scheme is achieved. The corresponding MAP prior shape estimator is also proposed. Our approach requires a much simpler initialization and has a lower computational complexity than the other popular methods.

References

[1] J. S. Duncan and N. Ayache, "Medical image analysis: Progress over two decades and the challenges ahead," *IEEE Trans. Pattern Anal. Mach. Intell.*, vol. 22, no. 1, pp. 85–106, Jan. 2000.
[2] T. McInerney and D. Terzopoulos, "Deformable models in medical image analysis: A survey," *Med. Image Anal.*, vol. 1, no. 2, pp. 91–108, 1996.
[3] M. Kass, A. Witkin, and D. Terzopoulos, "Snakes: Active contour models," *Int. J. Comput. Vis.*, vol. 1, no. 4, pp. 321–331, 1987.
[4] V. Caselles, F. Catte, T. Coll, and F. Dibos, "A geometric model for active contours," *Numerische Mathematik*, vol. 66, pp. 1–31, 1993.
[5] R. Malladi, J. A. Sethian, and B. C. Vermuri, "Shape modeling with front propagation: A level set approach," *IEEE Trans. Pattern Anal. Mach. Intell.*, vol. 17, no. 2, pp. 158–174, Feb. 1995.
[6] V. Caselles, R. Kimmel, and G. Sapiro, "Geodesic active contours," *Int. J. Comput. Vis.*, vol. 22, no. 1, pp. 61–79, 1997.

[7] S. Osher and J. A. Sethian, "Fronts propagating with curvature-dependent speed: Algorithms based on Hamilton-Jacobi formulations," *J. Comput. Phys.*, vol. 79, pp. 12–49, 1988.

[8] J. A. Sethian, *Level Set Methods and Fast Marching Methods*, 2nd ed. New York: Cambridge Univ. Press, 1999.

[9] J. Suri, K. Liu, S. Singh, S. Laxminarayana, and L. Reden, "Shape recovery algorithms using level sets in 2-D/3-D medical imagery: A state-of-the-art review," *IEEE Trans. Inf. Technol. Biomed.*, vol. 6, no. 1, pp. 8–28, Mar. 2002.

[10] L. D. Cohen and R. Kimmel, "Global minimum for active contour models: A minimal path approach," *Int. J. Comput. Vis.*, vol. 24, pp. 57–78, 1997.

[11] L. D. Cohen and T. Deschamps, "Grouping connected components using minimal path techniques," in *Proc. IEEE Comput. Soc. Conf. CVPR*, 2001, pp. 102–109.

[12] C. Han, T. S. Hatsukami, J.-N. Hwang, and C. Yuan, "A fast minimal path active contour model," *IEEE Trans. Image Process.*, vol. 10, no. 6, pp. 865–873, Jun. 2001.

[13] T. F. Cootes, C. J. Taylor, D. H. Cooper, and J. Graham, "Active shape models—Their training and application," *Comput. Vis. Image Understand.*, vol. 61, no. 1, pp. 38–59, Jan. 1995.

[14] L. H. Staib and J. S. Duncan, "Boundary finding with parametrically deformable models," *IEEE Trans. Pattern Anal. Mach. Intell.*, vol. 14, no. 11, pp. 1061–1075, Nov. 1992.

[15] M. E. Leventon, W. E. L. Grimson, and O. Faugeras, "Statistical shape influence in geodesic active contours," in *Proc. IEEE Comput. Soc. Conf. CVPR*, Jun. 2000, vol. 1, pp. 316–323.

[16] Y. Chen, S. Thiruvenkadam, H. D. Tagare, F. Huang, D. Wilson, and E. A. Geiser, "On the incorporation of shape priors into geometric active contours," in *Proc. IEEE Workshop Variational Level Set Methods Comput. Vis.*, 2001, pp. 145–152.

[17] P. Yan and A. A. Kassim, "Medical image segmentation with minimal path deformable models," in *Proc. IEEE ICIP*, Singapore, Oct. 2004, pp. 2733–2736.

[18] R. Deriche, J. P. Cocquerez, and G. Almouzni, "An efficient method to build early image description," in *Proc. Int. Conf. Pattern Recogn.*, Rome, Italy, 1988, pp. 588–591.

[19] A. Martelli, "An application of heuristic search methods to edge and contour detection," *Graph. Image Process.*, vol. 19, no. 2, pp. 73–83, 1976.

[20] J. K. Udupa, P. K. Saha, and R. A. Lotufo, "Boundary detection via dynamic programming," in *Proc. SPIE Med. Imaging*, 1992, vol. 1808, pp. 33–39.

[21] H. Breu, J. Gil, D. Kirkpatrick, and M. Werman, "Linear time euclidean distance transform algorithms," *IEEE Trans. Pattern Anal. Mach. Intell.*, vol. 17, no. 5, pp. 529–533, May 1995.

[22] E. L. Ritman, R. A. Robb, and L. D. Harris, *Imaging Physiologic Functions: Experience With the Dynamic Spatial Reconstructor*. New York: Praeger, 1985.

[23] J. Canny, "A computational approach to edge detection," *IEEE Trans. Pattern Anal. Mach. Intell.*, vol. 8, no. 6, pp. 679–698, Nov. 1986.

[24] A. A. Amini, T. E. Weymouth, and R. C. Jain, "Using dynamic programming for solving variational problems in vision," *IEEE Trans. Pattern Anal. Mach. Intell.*, vol. 12, no. 9, pp. 855–866, Sep. 1990.

[25] C. Cocosco, V. Kollokian, R.-S. Kwan, and A. Evans, "BrainWeb: Online interface to a 3D MRI simulated brain database," in *Proc. 3rd Int. Conf. Functional Mapping Human Brain*. Copenhagen, Denmark, May 1997, vol. 5, p. 425.

Pingkun Yan (S'04–M'06) received the B.Eng. degree in electronics engineering from the University of Science and Technology of China, Hefei, China, in 2001, and the Ph.D. degree in electrical and computer engineering from the National University of Singapore, Singapore, in 2005.

Since June 2005, he has been a Research Associate with the Computer Vision Laboratory, School of Computer Science, University of Central Florida, Orlando. His research interests include medical image analysis, computer vision, biomedical information technology, image processing, and compression.

Dr. Yan is a member of the IEEE Computer Society and Medical Image Computing and Computer Assisted Intervention (MICCAI) Society. He was the recipient of the MICCAI 2005 Student Award for the best presentation on image segmentation and analysis at the 8th International Conference on MICCAI, 2005. P. Yan joined IEEE as a student member in 2004. He has been an IEEE member since 2006.

Ashraf A. Kassim (S'82–M'85) received the B.Eng. (first class honors) and M.Eng. degrees in electrical engineering from the National University of Singapore (NUS), Singapore, in 1985 and 1987, respectively, and the Ph.D. degree in electrical and computer engineering from Carnegie Mellon University, Pittsburgh, PA, in 1993.

From 1986 to 1988, he was with Texas Instruments. Since 1993, he has been with the Electrical and Computer Engineering Department, NUS, where he is currently an Associate Professor and the Vice Dean of the Engineering Faculty. His research interests include image analysis, machine vision, video/image processing, and compression.